Harvesting Low Molecular Weight Biomarkers Using Gold Nanoparticles

Luai R. Khoury,[†] Riki Goldbart,[‡] Tamar Traitel,[‡] Giora Enden,[*,†] and Joseph Kost[*,‡]

[†]Department of Biomedical Engineering, Ben-Gurion University of the Negev, Beer Sheva, 8410501, Israel and [‡]Department of Chemical Engineering, Ben-Gurion University of the Negev, Beer Sheva, 8410501, Israel

ABSTRACT We developed and characterized a platform based on gold (Au) nanoparticles (NPs) coated with poly(acrylic acid) (PAA) for harvesting positively charged, low molecular weight (LMW) proteins. The particles are synthesized using a layer by layer (LbL) procedure: first the gold NPs are coated with positively charged polyethylenimine (PEI) and subsequently with PAA. This simple procedure produces stable PAA-PEI-Au (PPAu) NPs with high selectivity and specificity. PPAu NPs successfully harvested, separated, and detected various LMW proteins and peptides from serum containing a complex mixture of abundant high molecular weight (HMW) proteins, including bovine serum albumin (BSA) and Immunoglobulin G (IgG). In addition, PPAu NPs selectively harvested and separated LMW proteins from serum in the presence of another positively charged competing protein. Furthermore, PPAu NPs successfully harvested a LMW biomarker in a mock diseased state. This system can be applied in various biomedical applications where selective harvesting and identifying of LMW proteins is required. A particularly useful application for this system can be found in early cancer diagnosis as described hereinafter.

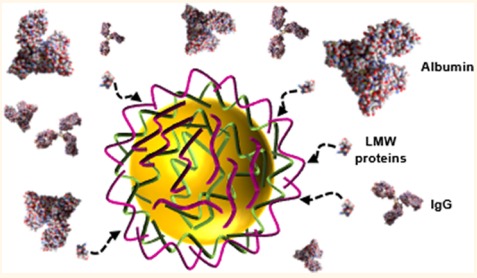

KEYWORDS: gold nanoparticles · layer by layer · biomarker harvesting · cancer diagnosis

The efficacy of cancer treatment depends on the pathological state of the disease; the earlier the detection and diagnosis, the more efficient will the treatment be. Several methods are commonly used to detect cancer such as computed axial tomography (CAT) scan,[1] ultrasound[2] and biopsy[3] to mention a few. These methods might lead to false negative diagnosis because of their limited resolution at the early stages of the tumor (CAT scan and ultrasound) or might be risky to the patient because of their invasive nature (biopsy). The lack of early stage diagnostic tools has stimulated a pursuit for alternative approaches.[4,5] One of the most promising approaches is based on the fact that tumor cells excrete low molecular weight (LMW) biomolecules (<10 kDa) to the bloodstream that are specific to the tumor type at a rate proportional to the tumor age/size.[6,7] Harvesting, concentrating, and analyzing these biomarkers can provide valuable diagnostic information.[8] However, a few drawbacks hinder the immediate and direct utilization of this approach. The major obstacle in selective harvesting of LMW biomarkers from the blood and analyzing them is their low abundance.[7] Proteolysis by blood-plasma proteases further lowers the concentration of these proteins and decreases their detectability.[9] In addition, carrier proteins (*e.g.*, albumin and immunoglobulin (IgG)) exist at concentrations billion-fold higher than those of the biomarkers thereby masking the LMW biomarkers and hindering their detection.[10] As a result several sample preparations are needed for mass spectrometry (MS) to filter out the high molecular weight (HMW) proteins.[11] However, recent studies showed that LMW biomarkers are associated noncovalently with HMW protein.[12] Therefore, removing HMW proteins from the sample may further dilute the samples from LMW biomarkers and exhibit false negative results.[9]

Most conventional method laboratories do not carry instruments with sufficient accuracy, precision, resolution and sensitivity to perform adequate measurements to directly detect low concentrations of LMW biomarkers in blood samples. The NP-based harvesting system that has been developed in this research offers means to overcome the aforementioned obstacles.

* Address correspondence to genden@bgu.ac.il, kost@bgu.ac.il.

Received for review December 30, 2014 and accepted June 1, 2015.

Published online June 01, 2015
10.1021/nn507467y

Here we applied the layer-by-layer (LbL) method to coat gold NPs with PAA (pK = 3.5) whose carboxylic group served as a bait to rapidly harvest, concentrate and detect a positively charged LMW fraction of serum proteins (<10 kDa). The biomarker harvesting concept is based on the known evidence that the peptidome is a rich source of LMW biomarkers.[13−15] Gold NPs are widely employed in biomedical research in various areas, including drug delivery[16−23] and diagnostics.[24,25] They exhibit a series of favorable features as they are biocompatible, simple to prepare and size-controllable.[26] By coating them with different baits using the LbL method,[27,28] they can be functionalized to harvest different desired molecules displaying negligible diameter changes, a critical property of NPs in biomedical applications in general and LMW biomarker harvesting in particular.[29−35]

RESULTS AND DISCUSSION

Preparation and Characterization PPAu NPs. Here we first synthesized ∼14 nm diameter, naked, homogeneous and negatively charged Au NPs.[23] Next, according to the LbL method the naked NPs were coated with positively charged polyethylenimine (PEI) polymer (10 kDa), followed by coating with negatively charged PAA (8 kDa) (Scheme 1). Cryogenic transmission electron microscopy (cryo-TEM) images of naked (Figure 1A), and coated (Figure 1B) NPs provided their size distributions: Figure 1C and Figure 1D, respectively. The UV−vis spectra revealed that the PPAu remained predominantly disaggregated after each coating as the maximum of the plasmon peak shifted from 520 nm, through 522 to 524 nm representing the naked and the consecutively coated NPs, respectively (Figure 1E). These results were in agreement with mean cryo-TEM diameter readings of ∼14.5 nm after the final layer deposition (Figure 1B, D) showing no significant deviation from naked NPs (Figure 1A, C). Furthermore, the alternation of ζ-potential from −33.18 ± 5.47 mV, to +45.02 ± 1.31 mV, and then to −53.82 ± 4.28 mV, after the coating completion of each layer, confirmed the deposition of each polymer on the nanoparticle surface. (Figure 1F).

Monitoring SDFα Adsorption on PPAu NPs. SDFα protein (MW = 8 kDa, pI = 10.3) was chosen as a LMW protein model to demonstrate its adsorption to PPAu NPs. SDFα is of particular interest because of its association to cancer: it promotes different mechanisms in cellular transformation and tumor growth such as angiogenesis, tumor spreading and metastasis.[36] Recently, it was reported that SDFα plays a major role in a "chase and run" mechanism in cancer metastasis.[37] Furthermore, its detection is challenging because of its extremely low concentration (∼1.5 ng/mL) and short half-life time in the blood, less than 10 min.[36]

To monitor adsorption of SDFα on PPAu NPs, agarose gel electrophoresis (GE) (1%) was conducted (Figure 2C). 20 μL of PPAu NPs (5.86×10^{11} particles/mL) were incubated with various concentrations of SDFα solution (2.5−30 μg/mL) in 20 μL of 20 mM Tris-HCl (pH = 7) for 1 h at room temperature (RT). Agarose gel electrophoresis results showed that PPAu NPs' band (Figure 2C, lane 1) is clearly visible in the gel and shows larger mobility than that of PPAu NPs incubated with SDFα (2.5−30 μg/mL) in lanes 2−6 (Figure 2A). The mobility reductions in lanes 2−6 are attributed to the particles' size increase and to the ζ-potential decrease, or to the Debye length increase when the size and charge are unchangeable.[38] SDFα adsorption on the PPAu NP surface weakens the electrostatic repulsion between the NPs while allowing the van der Waals attraction to become dominant and generate larger aggregates. In addition, the decrease in the ζ-potential reduces the driving force acting on the NPs. As a result, a broader distribution of NP sizes is obtained as reflected by the band smear in lane 5. In Figure 2C lane 6, PPAu-SDFα complexes remained stuck in the gel well, probably because of the formation of large aggregates and the reduction of the ζ-potential. However, incubation of naked Au and PEI-Au NPs with various concentrations of SDFα did not lead to mobility differences between bands as shown in Figure 2B, and slight mobility differences between bands in Figure 2A. SDFα either escaped from the gel due to its small size or adsorbed to the NPs' surfaces (Figure 2A, lane 6). This suggested that SDFα did not adsorb to PEI-Au or to the surface of naked Au NPs as in PPAu NPs. It was therefore concluded that PAA was the cause for SDFα adsorption. The aggregate hypothesis was supported by Cryo-TEM images of samples used in the GE showing that the PPAu NPs were enclosed

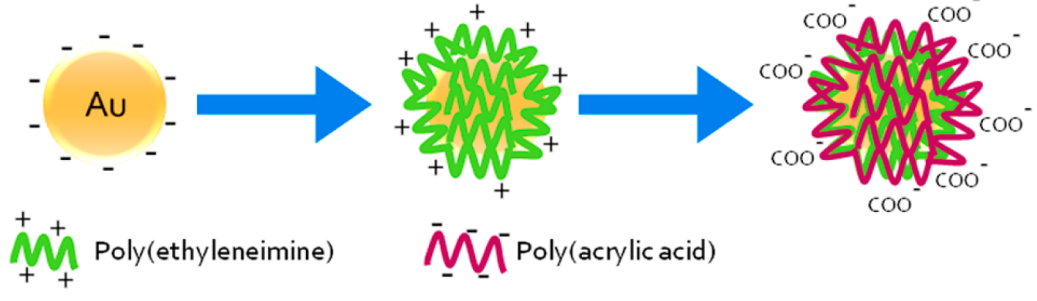

Scheme 1. Schematic description of the LbL strategy to functionalize Au nanoparticles.

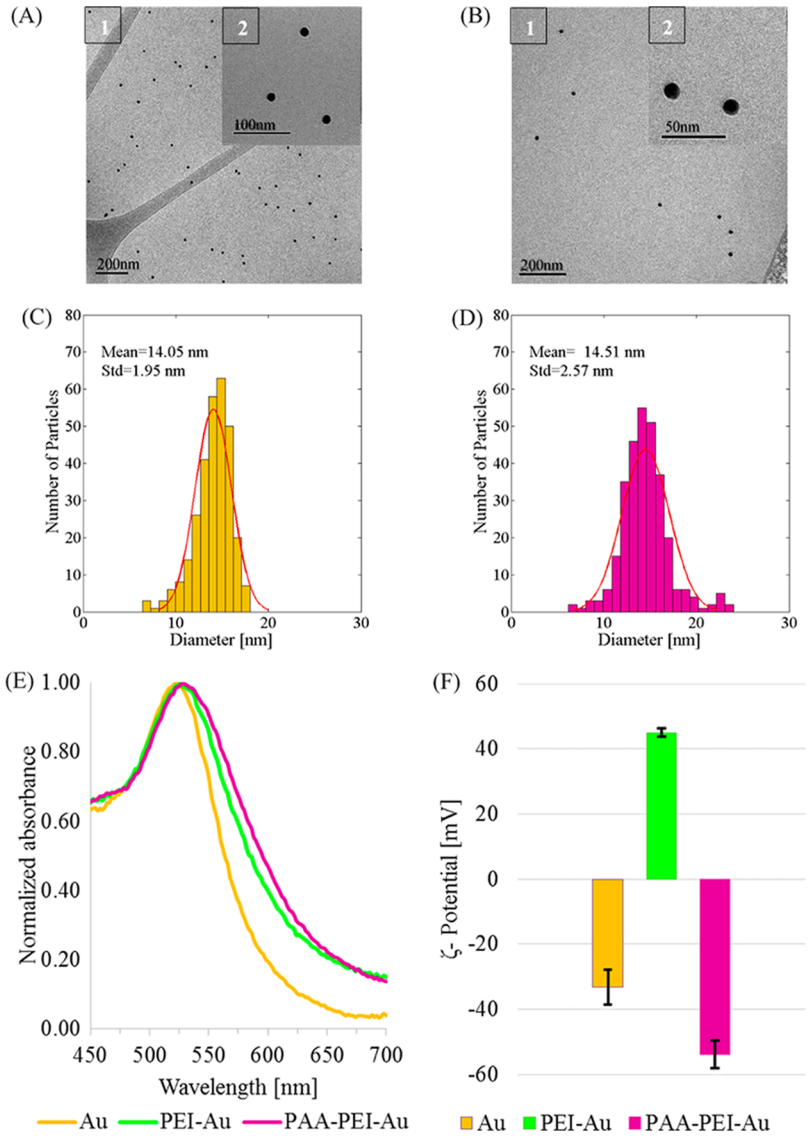

Figure 1. (A1) and (B1) cryo-TEM images of Au NPs and PPAu NPs, respectively (Bar indicates 200 nm); (A2) and (B2) magnified cryo-TEM images of Au NPs and PPAu NPs, respectively; (C) and (D) size distribution histograms of naked Au NPs and PPAu NPs, respectively; (E) evolution of the ζ-potential *versus* the number of layers on the Au NPs. (F) UV−visible spectra of naked Au NPs and coated Au NPs with different layers.

within a protein SDFα matrix designated by the arrow in Figure 2D. Notably, larger aggregates were formed by increasing the SDFα concentration. Other studies on the effects of protein adsorption on Au NPs showed similar formations of protein−NP complexes.[39]

LMW Biomarker Harvesting by PPAu Nanoparticles. Two independent methods were applied to assess the harvesting potential of PPAu NPs: sodium dodecyl sulfate-polyacrylamide gel electrophoresis (SDS-PAGE) and fluorescence measurements. In the first method, SDFα (10 μg/mL) was incubated with fetal bovine serum (FBS) (50%) for 1 h at room temperature (RT). FBS was chosen because it contains more than 3700 positively and negatively charged proteins and therefore simulates an *in vivo* situation.[40] After SDFα incubation with FBS, PPAu NPs (5.86×10^{11} NPs/mL) were added to the solution, and incubated for 1 h at RT, then washed and centrifuged three times (Scheme 2). The NPs and supernatant were both loaded on the gel, demonstrating the NPs' capacity to harvest and concentrate most of the SDFα and separate most of it from the rest of the solution in one step (Figure 3: lanes (4) and (5)), leaving out all the HMW proteins. From lane (1), we can see that FBS has several HMW proteins that exist in high concentrations (*e.g.*, albumin 66 kDa, IgG 25 kDa).[41]

In the second fluorescence-based method PPAu and naked Au NPs dispersions were incubated separately with FITC-labeled peptide (PK (FK) 5P), MW 2219.70 Da and p*I* = 11.50 which was previously incubated with FBS, then washed and centrifuged three times as in the former method (Scheme 2). The fluorescent intensity of the supernatant was measured using fluorometer. The FITC-peptide in FBS served as

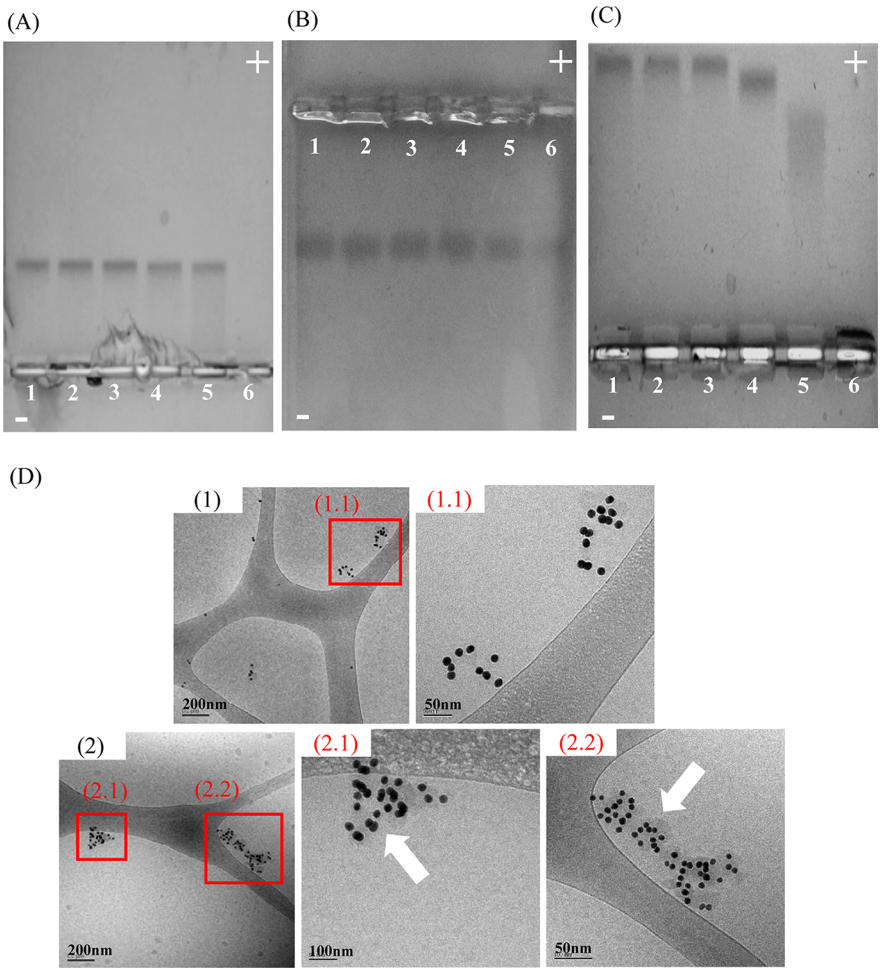

Figure 2. (A–C) Agarose gel (1%) electrophoresis of (A) Naked Au NPs with 0, 2.5, 5, 10, 20 μg/mL SDFα, (lanes 1–5, respectively), SDFα without NPs (lane 6); (B) PEI-Au NPs with 0, 2.5, 5, 10, 20, and 30 μg/mL SDFα, (lanes 1–6, respectively); (C) PPAu NPs with 0, 2.5, 5, 10, 20, and 30 μg/mL SDFα, (lanes 1–6, respectively); (D) cryo-TEM images of PPAu-SDFα complexes: (1) 20 μg/mL SDFα; (2) 30 μg/mL SDFα. Insets (1.1), (2.1), and (2.2) are magnifications of the rectangular domains in (1) and (2). White arrows point at the SDFα matrix.

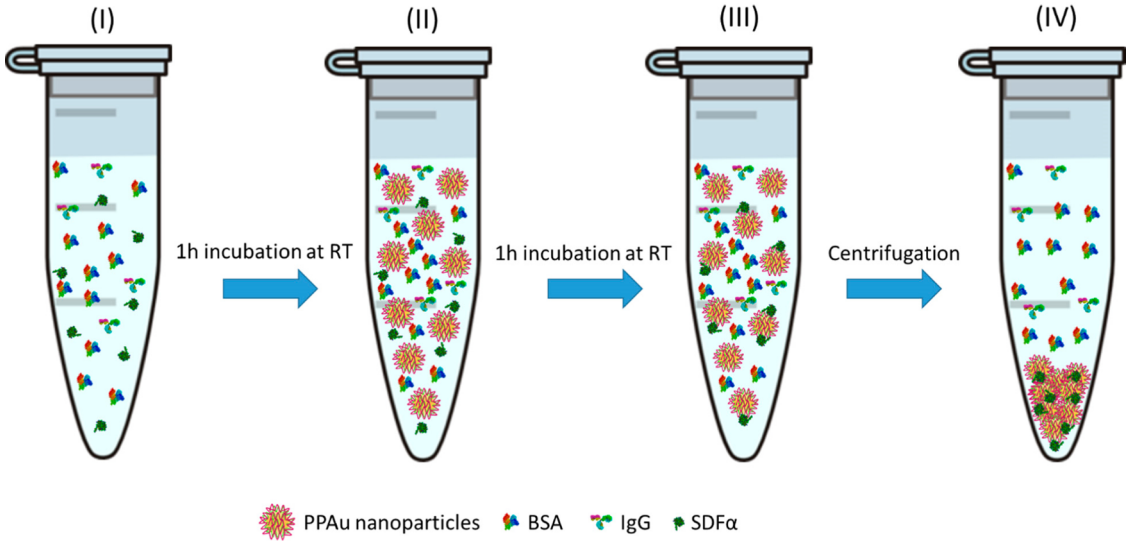

Scheme 2. A schematic illustration of harvesting SDFα from FBS by PPAu NPs. (I) LMW biomarker incubated with FBS; (II) PPAu NPs added to FBS and LMW biomarker; (III) LMW biomarker adsorbed on PPAu NPs; (IV) PPAu NPs separated by centrifugation from the dispersion for analysis.

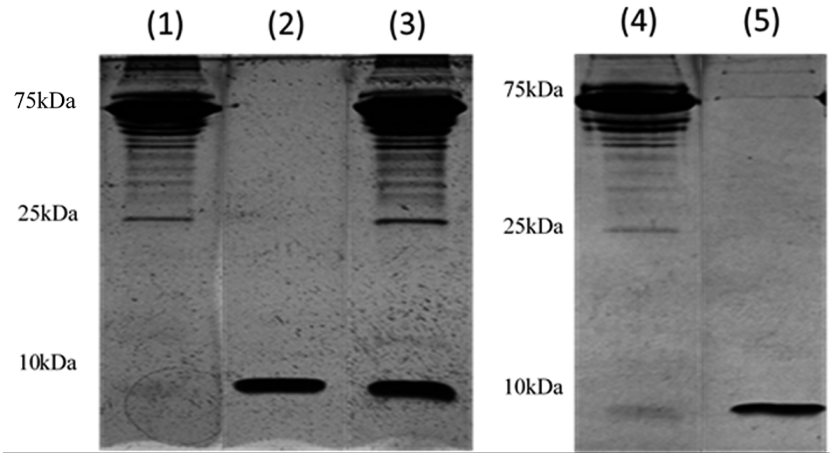

Figure 3. SDS-PAGE analysis showing SDFα harvesting by PPAu NPs: (1) FBS; (2) SDFα; (3) SDFα+ FBS (4) supernatant; (5) SDFα harvested by PPAu NPs.

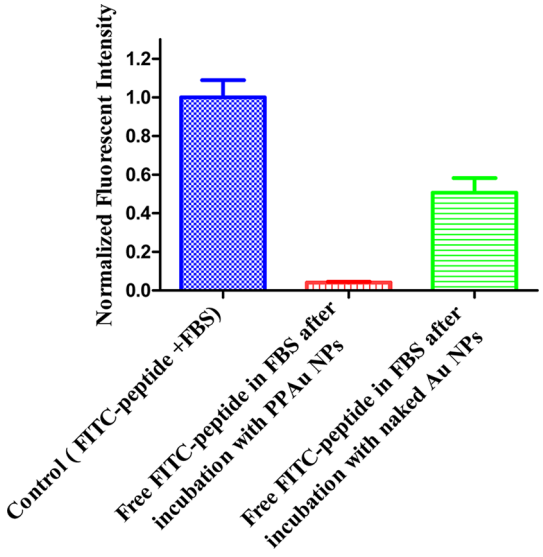

Figure 4. Mean normalized fluorescent intensity values of FITC-labeled peptide (PK(FK)5P) in FBS solution (blue); Free FITC-labeled peptide (PK(FK)5P) in supernatant after PPAu separation (green); Free FITC-labeled peptide (PK(FK)5P) in supernatant after naked Au NPs separation (red) (three replicate analyses and standard deviation are shown).

control for the fluorescent signal, and the FBS served as control for the background signal. It can be seen (Figure 4) that the remaining peptide in the supernatant is significantly less (~4%) than its initial amount in the control after incubation with PPAu NPs. On the other hand, in the case of naked Au NPs, approximately half of FITC-peptide is free in the sample. These results indicate that FITC-labeled peptide has larger affinity to PPAu than to naked Au NPs suggesting the significant reduction in the fluorescent intensity is due to binding on NPs surface and not as a result of FITC molecule quenching by gold. The reduction in fluorescence intensity of naked Au NPs is not surprising given the charge of naked Au NPs (Figure 4).

To assess the selectivity of PPA NPs to LMW biomarkers (<10 kDa), Platelet Derived Growth Factor B (PDGF B) (14.4 kDa, p*I* = 9.4) was chosen as a competing, positively charged model biomarker.[42−44] PDGF B was incubated with FBS for 1 h at RT and then PPAu NPs were added to the solution. The solution was washed and centrifuged three times after which the PPAu NPs and the supernatant were loaded on gel lanes. As seen in Figure 5, a minor amount (~30%) of the entire PDGF B is harvested by PPAu NPs (lane 5), indicating that the affinity of PPAu to proteins with molecular weight (MW) higher than 10 kDa is low compared to that of SDFα and FITC-labeled peptide which were totally harvested from the serum.

An experiment was conducted to demonstrate the selectivity of PPAu NPs to LMW cationic peptides. Trypsin solution at a concentration of 0.62×10^{-6} M was incubated with PPAu NPs (5.86×10^{11} NPs/mL) for 1 h at RT. Then, the dispersion was centrifuged and the supernatant was saved. The concentrations of free trypsin in the solution and in the control samples were quantified using micro-bicinchoninic acid (mBCA) assay. In Figure 6 it can be seen that the concentration of free trypsin in the solution after incubation with PPAu NPs has not changed compared to the control sample of trypsin ($p = 0.41$). This suggests that the selective harvesting property of the PPAu NPs is a resultant of two factors: their electric charge and their attraction to LMW proteins. It is hypothesized that fine-tuning the combinations of these factors may increase the resolution of the captures and provide reliable diagnostic tools.

Another experiment was conducted to assess the harvesting potential of PPAu NPs in the presence of two different positively charged proteins and FBS. SDFα, PDGF B and FBS were incubated together, and then PPAu NPs were added to the solution. The SDS-PAGE procedure was carried out as described above. In Figure 7 at lane 3 we see that PPAu NPs harvest most of the SDFα in the solution and only a minute fraction of the PDGF B. The remaining FBS proteins and PDGF B

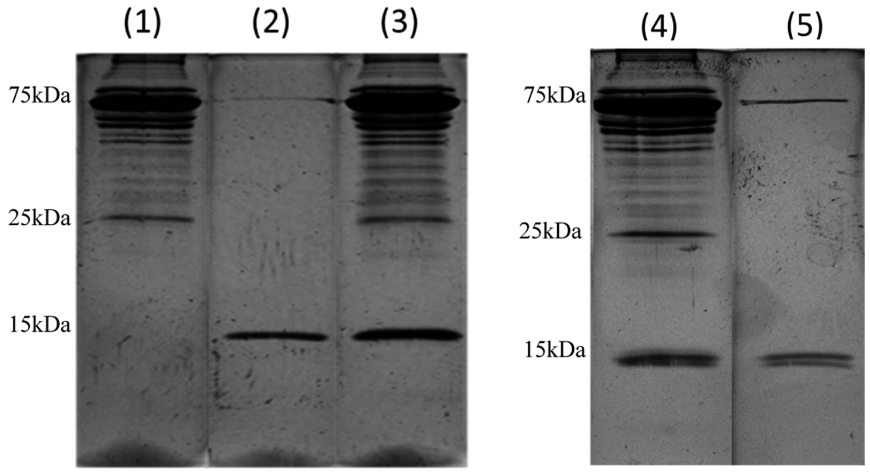

Figure 5. SDS-PAGE analysis showing PDGF B partial harvesting from FBS by PPAu nanoparticles in (1) FBS; (2) PDGF B; (3) FBS+PDGF B; (4) supernatant; (5) PDGF B harvested by PPAu nanoparticles.

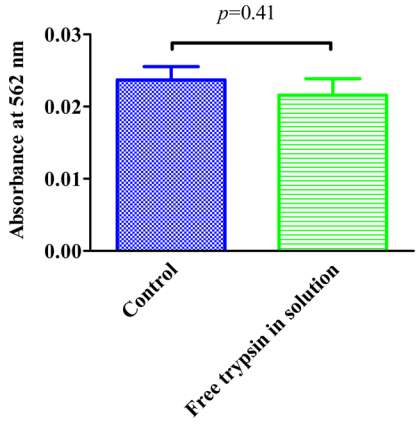

Figure 6. mBCA readings of control solution of trypsin (0.023 ± 0.001) and free trypsin in a solution after its incubation with PPAu NPs (0.021 ± 0.002).

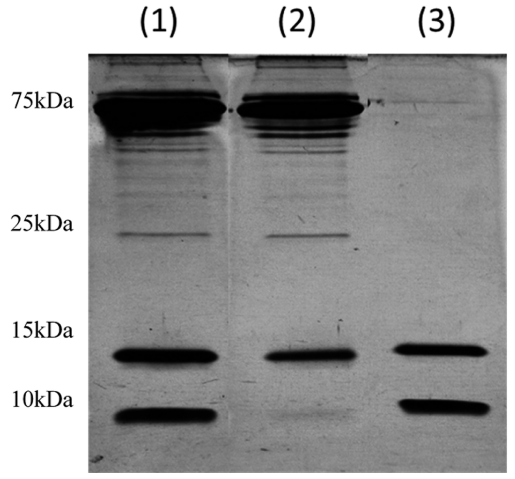

Figure 7. SDS-PAGE results showing the harvesting of SDFα from FBS by PPAu nanoparticles in the presence of a positively charged protein PDGF B: (1) FBS+PDGF B +SDFα; (2) Supernatant; (3) SDFα+PDGF B harvested by PPAu nanoparticles.

are left in the supernatant (lane 2) indicating that PPAu NPs harvest SDFα and LMW proteins from the serum selectively and effectively.

More experiments were done to assess the harvesting sensitivity of PPAu NPs at an extremely low concentration of SDFα in a mock diseased state. SDFα was incubated with FBS: [3.88 ng/mL] in the first experiment (Exp. 1) and [1.88 ng/mL] in the second (Exp. 2). Then, PPAu NPs (5.86×10^{11} NPs/mL) were added to the solution and were incubated for 1 h at RT. The entire dispersion was centrifuged and the supernatant was saved. The enzyme-linked immunosorbent assay (ELISA) procedure was used to evaluate the SDFα concentration in the supernatant and in the control samples.

In Figure 8 Exp. 1 we see that the concentration of SDFα in the supernatant was 3.13 ± 0.076 ng/mL compared to the control sample (3.88 ± 0.198 ng/mL, p = 0.006). This suggests that the remaining SDFα protein (0.75 ± 0.123 ng/mL) had adsorbed to the PPAu NPs' surfaces, which is above the detection threshold of the ELISA kit at hand (0.044 ng/mL). At the lower

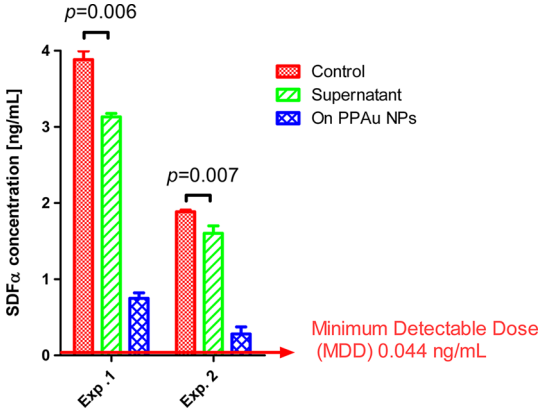

Figure 8. ELISA reading of control solution of FBS+ SDFα (3.88 ± 0.198 ng/mL, 1.88 ± 0.04 ng/mL) and SDFα concentration in supernatant (3.13 ± 0.076 ng/mL, 1.60 ± 0.169 ng/mL) and on PPAu NPs (0.75 ± 0.123 ng/mL, 0.28 ± 0.16) in Exp. 1 and Exp. 2, respectively.

concentration of SDFα (1.88 ng/mL) in Exp. 2, the concentration in the supernatant was 1.60 ± 0.169 ng/mL compared to that in the control sample (1.88 ± 0.04 ng/mL, $p = 0.007$), suggesting that the remaining SDFα protein had adsorbed to the PPAu NPs' surfaces.

In clinically relevant cases, after separation of the LMW proteins/peptides, the harvested molecules eluted from the PPAu NPs or the supernatant can be analyzed using other sensitive methods such as MALDI-TOF, which can identify and classify all LMW proteins/peptides. This approach is superior to conventional immunoassay platforms, such as antibody arrays and antibody-conjugated NPs which cannot effectively measure panels of analyte fragments. This is because immunoassays rely on antibody-based capture and detection methods. Antibody-based methods cannot distinguish the parental molecule from its cleaved fragments because the antibody recognizes its cognate epitope in both the parent and the fragment molecules. Also, the variety and large number of protein fragments that exist in a sample might make their detection by antibody-conjugated NPs' system very complicated and challenging. Therefore, a method capable of harvesting, separating and concentrating LMW biomarkers from serum for future analysis is highly desired.

This selectivity may be attributed to the nanoparticle surface curvature, and to the functionalizing group on the PPAu nanoparticle surface. Researches have publicized that nanoparticle−protein interaction depends on the nanoparticle surface curvature.[29−31,34,45] Deng *et al.* showed that decreasing the nanoparticles' diameters leads to a decrease in the adsorption dynamics between large proteins (*e.g.*, fibrinogen) and nanoparticles.[45] Lundqvist *et al.* showed that HCAII (~30 kDa) protein adsorbed more firmly to larger particles than to smaller ones.[30] The above and other researches confirm our results by demonstrating that protein adsorption is affected by nanoparticle morphology due to steric hindrance, where they showed that smaller proteins preferably adsorbed to highly curved nanoparticle. Furthermore, they showed that decreasing the nanoparticle curvature (to nearly flat surfaces) enhances the adsorption of the large proteins to nanoparticle surfaces.[31,46] These results demonstrate the adsorption of LMW proteins, the partially adsorption of PDGF Bon PPAu NPs' surfaces, and the exclusion of other HMW proteins existing in serum.

CONCLUSIONS

In summary, we successfully demonstrated that poly(acrylic acid) coated gold NPs created by the LbL method can be used to selectively harvest positively charged LMW biomarkers (<10 kDa) such as SDFα and FITC-labeled peptide in one step. The harvesting process takes place in the presence of other positively charged biomarkers such as PDGF B (>10 kDa) while leaving out abundant proteins such as albumin and IgG. This novel NP system has many advantages, including simple self-assembly synthesis, high stability and excellent binding specificity. Moreover, these NPs might probably be functionalized by different layering to harvest, concentrate and detect different molecules.

EXPERIMENTAL METHODS

PPAu Synthesis. Citrate capped gold nanoparticles were prepared according to a published procedure.[1] Chloroauric acid ($HAuCl_4$) stock solution (19 mL, 0.25 mM) was boiled with vigorous stirring. Then, 1 mL of sodium citrate (0.5%) was added to the boiled solution. The gold solution gradually forms as the citrate reduces the gold(III) to neutral gold atoms and gold gradually starts to precipitate in the form of subnanometer particles. Then the solution was boiled for further 30 min with vigorous stirring. A progressive color change was observed from yellowish toward red. The Au nanoparticles were characterized by cryogenic transmission electron microscopy (cryo-TEM), UV−visible spectroscopy (UV−vis), ζ-potential.

PEI-Au. PEI-Au was prepared using commercially available PEI (10 kDa). PEI cationic polymer was dissolved in ddH_2O (100 mg/mL) and stirred; previously prepared citrate−capped gold nanoparticle solution was added dropwise to the polymer solution and the solution was stirred overnight. PEI-Au nanoparticles were purified by high speed centrifugation and redispersed in ddH_2O; the process was repeated three times. The PEI-Au nanoparticles were characterized by UV−vis, and ζ-potential.

PAA-PEI-Au. PAA-PEI-Au was prepared using commercially available PAA (8 kDa). PAA anionic polymer was dissolved in ddH_2O, PEI-Au nanoparticle solution was added dropwise to the polymer solution and the solution was stirred overnight. PAA-PEI-Au nanoparticle were purified by high speed centrifugation and redispersed in ddH_2O; the process was repeated three times. The PAA-PEI-Au nanoparticles were characterized by cryo-TEM, UV−vis, ζ-potential.

Cryo-TEM. Au and PPAu solution samples were prepared on a copper grid coated with a perforated lacy carbon 300 mesh (Ted Pella Inc.). A typically 4 μL drop from the solution was applied to the grid and blotted with a filter paper to form a thin liquid film of solution. The blotted sample was immediately plunged into liquid ethane at its freezing point (−183 °C). The procedure was performed automatically in the Plunger (Lieca EM GP). The vitrified specimens were transferred into liquid nitrogen for storage. The samples were studied using a FEI Tecnai 12 G2 TEM, at 120 kV with a Gatan cryo-holder maintained at −180 °C, and images were recorded on a slow scan cooled charge-coupled device CCD camera Gatan manufacturer. Images were recorded with the Digital Micrograph software package at low dose conditions to minimize electron beam radiation damage.

ζ-Potential. The surface charge of the naked Au, PEI-Au, and PAA-PEI-Au nanoparticles was evaluated by their ζ-potential. U-tube cuvette (DTS1060C, Malvern) for ζ-potential measurements by Zetasizer (ZN-NanoSizer, Malvern, England) was used. Each of the naked Au, PEI-Au, and PAA-PEI-Au nanoparticle samples were measured in automatic mode, at 25 °C, and the Smoluchowski model was used to calculate the zeta potential. For each sample the ζ-potential value was presented as the average value of three runs.

UV−Vis Spectra. UV−vis spectra of Au, PEI-Au, and PAA-PEI-Au were recorded using an infinite M200 spectrophotometer (TECAN) equipped with a temperature controller.

SDFα Adsorption on PPAu Nanoparticle. To monitor SDFα (8 kDa, p*I* 10.3) adsorption on PPAu nanoparticles, the peptide was incubated with constant concentration of PPAu nanoparticles while the peptide's concentration was varied from 0 to 30 μg/mL. The adsorption process was characterized by Agarose gel, and cryo-TEM

Agarose Gel. Agarose gel (1%) was used to monitor adsorption of SDFα on PPAu, PEI-Au, and on naked Au NPs. 20 μL of each PPAu and PEI-Au NPs dispersions (5.86×10^{11} NPs/mL) were incubated with solutions of SDFα at various concentrations (2.5, 5, 10, 20, and 30 μg/mL) in 20 μL of 20 mM Tris-HCl pH = 7 for 1 h at room temperature (RT). 20 μL of naked Au NPs dispersions were incubated with SDFα solutions at various concentrations (2.5, 5, 10, and 20 μg/mL in 20 μL of 20 mM Tris-HCl pH = 7), and the sixth well was used as a control for SDFα (20 μg/mL). Subsequently, 8 μL of loading dye was added to each sample, and the entire mixture was loaded into the gel's wells (40 μL size). A constant voltage (90 V) was applied for 25 min to ensure sufficient separation. The gel was stained by Coomassie Blue for 2 h, followed by water wash (200 mL) until protein bands were clear.

Cryo-TEM. The same samples used in agarose gel of PPAu, and PPAu + SDFα (20 μg/mL and 30 μg/mL) complexes were prepared on a copper grid coated with a perforated lacy carbon 300 mesh (Ted Pella Inc.). A typically 4 μL drop from the solution was applied to the grid and blotted with a filter paper to form a thin liquid film of solution. The blotted samples were immediately plunged into liquid ethane at its freezing point (−183 °C). The procedure was performed automatically in the Plunger (Lieca EM GP). The vitrified specimens were transferred into liquid nitrogen for storage. The samples were studied using a FEI Tecnai 12 G2 TEM, at 120 kV with a Gatan cryo-holder maintained at −180 °C. Images were recorded on a slow scan cooled charge-coupled device CCD camera Gatan manufacturer and recorded with the Digital Micrograph software package, at low dose conditions, to minimize electron beam radiation damage.

LMW Biomarker Harvesting by PPAu Nanoparticles. To test the ability of PPAu nanoparticles to harvest LMW biomarkers, SDFα, FITC-labeled (PK (FK)5PK, and PDGF B were incubated with fetal bovine serum (FBS) and PPAu nanoparticles as described below. Two methods were conducted to evaluate the PPAu nanoparticles harvesting performance: sodium dodecyl sulfate-polyacrylamide gel electrophoresis (SDS-PAGE) and fluorescence measurement.

SDS-PAGE. 10 μL of FBS (1:25 diluted in Tris-HCl 20 mM pH = 7) and 10 μL SDFα (10 μg/mL) at 20 mM of Tris-HCl pH = 7) were incubated for 1 h. Then, 20 μL of PPAu (5.86×10^{11}particles/mL) nanoparticles were incubated with the above FBS+SDFα solution for 1 h at RT. After incubation, samples were centrifuged at 10000*g* for 10 min at 4 °C and washed three times, and the supernatant was saved. Particles and supernatant derived from particle incubation were loaded on 15% Tris-Gel. PPAu nanoparticles were stacked in the stacking gel while adsorbed proteins were eluted from the particles in resolving gel. Proteins' bands were detected using silver staining.

10 μL FBS (1:25 diluted in Tris-HCl 20 mM) and 10 μL of PDGF B (10 μg/mL at 20 mM of Tris-HCl pH = 7) were incubated at RT for 1 h. Then, 20 μL of PPAu (5.86×10^{11}particles/mL) nanoparticles were incubated with the above FBS+ PDGF B solution for 1 h at RT. After incubation, samples were centrifuged at 10000*g* for 10 min at 4 °C and washed three times, and the supernatant was saved. Particles and supernatant derived from particle incubation were loaded on 15% Tris-Gel. PPAu nanoparticles were stacked in the stacking gel while adsorbed proteins were eluted from the particles in resolving gel. Proteins' bands were detected using silver staining.

To monitor the harvesting of SDFα in the presence of PDGF B by PPAu nanoparticles SDS-PAGE was applied. 10 μL FBS (1:25 diluted in Tris-HCl 20 mM) and 5 μL of each protein (0.625 μM, SDFα and PDGF B at 20 mM of Tris-HCl pH = 7) was incubated at RT for 1 h. 20 μL of PPAu (5.86×10^{11} NPs/mL) NPs were incubated with the above solution (FBS+SDFα+PDGF B) for 1 h at RT. After incubation, samples were centrifuged 10000*g* at 4 °C and washed three times, and the supernatant was saved. Particles and supernatant derived from particle incubation were loaded on 15% Tris-Gel. PPAu nanoparticles were stacked in the stacking gel while adsorbed proteins were eluted from the particles in resolving gel. Proteins' bands were detected using silver staining.

Fluorescent Measurement. Triplicate of 20 μL FBS (1:25 diluted in 20 mM Tris-HCl) and 20 μL of FITC-labeled (PK (FK) 5PK MW 2.219 kDa and p*I* 11.4 (10 μg/mL in 20 mM of Tris-HCl pH = 7) were incubated together for 1 h at RT. Then, 40 μL of PPAu and naked Au NPs (5.86×10^{11} NPs/mL) were incubated separately with the above FBS+FITC-labeled (PK (FK) solution for 1 h at RT. After incubation, samples were centrifuged 10000*g* at 4 °C, and the supernatant was measured in 96-well microplates using an infinite M200 spectrophotometer (TECAN) equipped with a temperature controller set at RT, 485 nm excitation and 519 nm emission. Triplicate of 50 μL of FBS (1:25 diluted in Tris-HCl 20 mM) of FITC-labeled (PK (FK) 5PK (10 μg/mL in 20 mM of Tris-HCl pH = 7) were used as control for the fluorescent signal, and FBS was used as a background signal.

Micro-Bicinchoninic Acid (mBCA) Assay. Triplicate of 40 μL of trypsin (MW 23.3 kDa, p*I* = 10.4) at concentrations of (0.62×10^{-6} M) and 40 μL PPAu NPs solution (5.86×10^{11} NPs/mL) were incubated for 1 h at RT. After incubation, samples were centrifuged 10000*g* at 4 °C, and 50 μL of supernatant was measured by using mBCA assay according to the manual instructions. Triplicate of 50 μL of Tris-HCl pH = 7 were used as control.

ELISA Measurements. Triplicates of 100 μL FBS (1:25 diluted in Tris-HCl 20 mM) and SDFα at different concentrations (Exp. 1 (3.88 ng/mL) and Exp. 2 (1.88 ng/mL)) in 20 mM of Tris-HCl pH = 7 were incubated together for 1 h at RT. Then, 50 μL of PPAu NPs (5.86×10^{11} NPs/mL) were incubated with 50 μL of each FBS+ SDFα solutions for 1 h at RT. After incubation, samples were centrifuged 10000*g* at 4 °C, and the supernatant was saved. 50 μL of supernatant was measured by using ELISA kit (R&D systems) according to the manual instructions. Triplicates of 50 μL FBS+SDFα were used as control at each concentration. The concentration of the SDFα in the samples was estimated by a calibration curve which was constructed using known concentrations of SDFα stock solutions.

Conflict of Interest: The authors declare no competing financial interest.

REFERENCES AND NOTES

1. Greenberg, A. K.; Lu, F.; Goldberg, J. D.; Eylers, E.; Tsay, J.; Yie, T.; Naidich, D.; McGuinness, G.; Pass, H.; Tchou-Wong, K.; *et al.* CT Scan Screening for Lung Cancer: Risk Factors for Nodules and Malignancy in a High-Risk Urban Cohort. *PLoS One* **2012**, *7*, e39403.
2. Zhi, H.; Ou, B.; Luo, B.; Feng, X.; Wen, Y.; Yang, H. Comparison of Ultrasound Elastography, Mammography, and Sonography in the Diagnosis of Solid Breast Lesions. *J. Ultrasound Med.* **2007**, *26*, 807–815.
3. Nelson, A. W.; Harvey, R. C.; Parker, R. A.; Kastner, C.; Doble, A.; Gnanapragasam, V. J. Repeat Prostate Biopsy Strategies after Initial Negative Biopsy: Meta-Regression Comparing Cancer Detection of Transperineal, Transrectal Saturation and MRI Guided Biopsy. *PLoS One* **2013**, *8*, e57480.
4. Geho, D. H.; Liotta, L. A.; Petricoin, E. F.; Zhao, W.; Araujo, R. P. The Amplified Peptidome: The New Treasure Chest of Candidate Biomarkers. *Curr. Opin. Chem. Biol.* **2006**, *10*, 50–55.
5. Liotta, L. A.; Ferrari, M.; Petricoin, E. Clinical Proteomics: Written in Blood. *Nature* **2003**, *425*, 905.
6. Mehta, A. I.; Ross, S.; Lowenthal, M. S.; Fusaro, V.; Fishman, D. A.; Petricoin, E. F.; Liotta, L. A. Biomarker Amplification by Serum Carrier Protein Binding. *Dis. Markers* **2003**, *19*, 1–10.
7. Deutsch, E. W.; Eng, J. K.; Zhang, H.; King, N. L.; Nesvizhskii, A. I.; Lin, B.; Lee, H.; Yi, E. C.; Ossola, R.; Aebersold, R. Human Plasma Peptide Atlas. *Proteomics* **2005**, *5*, 3497–3500.
8. Orvisky, E.; Drake, S. K.; Martin, B. M.; Abdel-Hamid, M.; Ressom, H. W.; Varghese, R. S.; An, Y.; Saha, D.; Hortin, G. L.; Loffredo, C. A.; *et al.* Enrichment of Low Molecular Weight Fraction of Serum for MS Analysis of Peptides Associated with Hepatocellular Carcinoma. *Proteomics* **2006**, *6*, 2895–2902.

9. Ayache, S.; Panelli, M.; Marincola, F. M.; Stroncek, D. F. Effects of Storage Time & Exogenous Protease Inhibitors on Plasma Proteins: Materials and Methods. *Am. J. Clin. Pathol.* **2006**, *126*, 174–184.
10. Lopez, M. F.; Mikulskis, A.; Kuzdzal, S.; Bennett, D. A.; Kelly, J.; Golenko, E.; DiCesare, J.; Denoyer, E.; Patton, W. F.; Ediger, R.; *et al.* High-Resolution Serum Proteomic Profiling of Alzheimer Disease Samples Reveals Disease-Specific, Carrier-Protein−Bound Mass Signatures. *Clin. Chem.* **2005**, *51*, 1946–1954.
11. Zhou, M.; Lucas, D. A.; Chan, K. C.; Issaq, H. J.; Petricoin, E. F.; Liotta, L. A.; Veenstra, T. D.; Conrads, T. P. An Investigation into the Human Serum "Interactome". *Electrophoresis* **2004**, *25*, 1289–1298.
12. Lowenthal, M. S.; Mehta, A. I.; Frogale, K.; Bandle, R. W.; Araujo, R. P.; Hood, B. L.; Veenstra, T. D.; Conrads, T. P.; Goldsmith, P.; Fishman, D.; *et al.* Analysis of Albumin-Associated Peptides and Proteins from Ovarian Cancer Patients. *Clin. Chem.* **2005**, *51*, 1933–1945.
13. Chung, L.; Moore, K.; Phillips, L.; Boyle, F. M.; Marsh, D. J.; Baxter, R. C. Novel Serum Protein Biomarker Panel Revealed by Mass Spectrometry and Its Prognostic Value in Breast Cancer. *Breast Cancer Res.* **2014**, *16*, R63–R63.
14. Sandanayake, N. S.; Camuzeaux, S.; Sinclair, J.; Blyuss, O.; Andreola, F.; Chapman, M. H.; Webster, G. J.; Smith, R. C.; Timms, J. F.; Pereira, S. P. Identification of Potential Serum Peptide Biomarkers of Biliary Tract Cancer Using MALDI MS Profiling. *BMC Clin. Pathol.* **2014**, *14*, 7–7.
15. Ueda, K.; Tatsuguchi, A.; Saichi, N.; Toyama, A.; Tamura, K.; Furihata, M.; Takata, R.; Akamatsu, S.; Igarashi, M.; Nakayama, M.; *et al.* Plasma Low-Molecular-Weight Proteome Profiling Identified Neuropeptide-Y as a Prostate Cancer Biomarker Polypeptide. *J. Proteome Res.* **2013**, *12*, 4497–4506.
16. Schneider, G.; Decher, G. Functional Core/Shell Nanoparticles *via* Layer-by-Layer Assembly. Investigation of the Experimental Parameters for Controlling Particle Aggregation and for Enhancing Dispersion Stability. *Langmuir* **2008**, *24*, 1778–1789.
17. Schneider, G.; Decher, G.; Nerambourg, N.; Praho, R.; Werts, M. H. V.; Blanchard-Desce, M. Distance-Dependent Fluorescence Quenching on Gold Nanoparticles Ensheathed with Layer-by-Layer Assembled Polyelectrolytes. *Nano Lett.* **2006**, *6*, 530–536.
18. Masereel, B.; Dinguizli, M.; Bouzin, C.; Moniotte, N.; Feron, O.; Gallez, B.; Vander Borght, T.; Michiels, C.; Lucas, S. Antibody Immobilization on Gold Nanoparticles Coated Layer-by-Layer with Polyelectrolytes. *J. Nanopart. Res.* **2011**, *13*, 1573–1580.
19. Boyer, C.; Bousquet, A.; Rondolo, J.; Whittaker, M. R.; Stenzel, M. H.; Davis, T. P. Glycopolymer Decoration of Gold Nanoparticles Using a LbL Approach. *Macromolecules* **2010**, *43*, 3775–3784.
20. Zheng, D.; Giljohann, D. A.; Chen, D. L.; Massich, M. D.; Wang, X.; Iordanov, H.; Mirkin, C. A.; Paller, A. S. Topical Delivery of siRNA-Based Spherical Nucleic Acid Nanoparticle Conjugates for Gene Regulation. *Proc. Natl. Acad. Sci. U. S. A.* **2012**, *109*, 11975–11980.
21. Boyer, C.; Whittaker, M. R.; Luzon, M.; Davis, T. P. Design and Synthesis of Dual Thermoresponsive and Antifouling Hybrid Polymer/Gold Nanoparticles. *Macromolecules* **2009**, *42*, 6917–6926.
22. Boyer, C.; Whittaker, M. R.; Chuah, K.; Liu, J.; Davis, T. P. Modulation of the Surface Charge on Polymer-Stabilized Gold Nanoparticles by the Application of an External Stimulus. *Langmuir* **2010**, *26*, 2721–2730.
23. Bousquet, A.; Boyer, C.; Davis, T. P.; Stenzel, M. H. Electrostatic Assembly of Functional Polymer Combs onto Gold Nanoparticle Surfaces: Combining RAFT, Click and LbL to Generate New Hybrid Nanomaterials. *Polym. Chem.* **2010**, *1*, 1186–1195.
24. Guo, C.; Boullanger, P.; Jiang, L.; Liu, T. Highly Sensitive Gold Nanoparticles Biosensor Chips Modified with a Self-Assembled Bilayer for Detection of Con A. *Biosens. Bioelectron.* **2007**, *22*, 1830–1834.
25. Phillips, R. L.; Miranda, O. R.; You, C.; Rotello, V. M.; Bunz, U. H. F. Rapid and Efficient Identification of Bacteria Using Gold-Nanoparticle-Poly(para-phenyleneethynylene) Constructs. *Angew. Chem., Int. Ed.* **2008**, *47*, 2590–2594.
26. Frens, G. Controlled Nucleation for the Regulation of the Particle Size in Monodisperse Gold Suspensions. *Nature (London), Phys. Sci.* **1973**, *241*, 20–22.
27. Gittins, D. I.; Caruso, F. Tailoring the Polyelectrolyte Coating of Metal Nanoparticles. *J. Phys. Chem. B* **2001**, *105*, 6846–6852.
28. Schneider, G.; Decher, G. From Functional Core/Shell Nanoparticles Prepared *via* Layer-by-Layer Deposition to Empty Nanospheres. *Nano Lett.* **2004**, *4*, 1833–1839.
29. Lundqvist, M.; Stigler, J.; Elia, G.; Lynch, I.; Cedervall, T.; Dawson, K. A. Nanoparticle Size and Surface Properties Determine the Protein Corona with Possible Implications for Biological Impacts. *Proc. Natl. Acad. Sci. U. S. A.* **2008**, *105*, 14265–14270.
30. Lundqvist, M.; Sethson, I.; Jonsson, B. Protein Adsorption onto Silica Nanoparticles: Conformational Changes Depend on the Particles' Curvature and the Protein Stability. *Langmuir* **2004**, *20*, 10639–10647.
31. Tenzer, S.; Docter, D.; Rosfa, S.; Wlodarski, A.; Kuharev, J.; Rekik, A.; Knauer, S. K.; Bantz, C.; Nawroth, T.; Bier, C.; *et al.* Nanoparticle Size Is a Critical Physicochemical Determinant of the Human Blood Plasma Corona: A Comprehensive Quantitative Proteomic Analysis. *ACS Nano* **2011**, *5*, 7155–7167.
32. Kaur, K.; Forrest, J. A. Influence of Particle Size on the Binding Activity of Proteins Adsorbed onto Gold Nanoparticles. *Langmuir* **2012**, *28*, 2736–2744.
33. Shang, W.; Nuffer, J. H.; Muñiz-Papandrea, V. A.; Colón, W.; Siegel, R. W.; Dordick, J. S. Cytochrome c on Silica Nanoparticles: Influence of Nanoparticle Size on Protein Structure, Stability, and Activity. *Small* **2009**, *5*, 470–476.
34. Roach, P.; Farrar, D.; Perry, C. C. Surface Tailoring for Controlled Protein Adsorption: Effect of Topography at the Nanometer Scale and Chemistry. *J. Am. Chem. Soc.* **2006**, *128*, 3939–3945.
35. Schäffler, M.; Sousa, F.; Wenk, A.; Sitia, L.; Hirn, S.; Schleh, C.; Haberl, N.; Violatto, M.; Canovi, M.; Andreozzi, P.; *et al.* Blood Protein Coating of Gold Nanoparticles As Potential Tool for Organ Targeting. *Biomaterials* **2014**, *35*, 3455–3466.
36. Vicari, A. P.; Caux, C. Chemokines in Cancer. *Cytokine Growth Factor Rev.* **2002**, *13*, 143–154.
37. Theveneau, E.; Steventon, B.; Scarpa, E.; Garcia, S.; Trepat, X.; Streit, A.; Mayor, R. Chase-and-Run between Adjacent Cell Populations Promotes Directional Collective Migration. *Nat. Cell Biol.* **2013**, *15*, 763–772.
38. Hou, J.; Szaflarski, D. M.; Simon, J. D. Quantifying the Association Constant and Stoichiometry of the Complexation between Colloidal Polyacrylate-Coated Gold Nanoparticles and Chymotrypsin. *J. Phys. Chem. B* **2013**, *117*, 4587–4593.
39. Zhang, D.; Neumann, O.; Wang, H.; Yuwono, V. M.; Barhoumi, A.; Perham, M.; Hartgerink, J. D.; Wittung-Stafshede, P.; Halas, N. J. Gold Nanoparticles Can Induce the Formation of Protein-based Aggregates at Physiological pH. *Nano Lett.* **2009**, *9*, 666–671.
40. Mahmoudi, M.; Lynch, I.; Ejtehadi, M. R.; Monopoli, M. P.; Bombelli, F. B.; Laurent, S. Protein−Nanoparticle Interactions: Opportunities and Challenges. *Chem. Rev.* **2011**, *111*, 5610–5637.
41. Tirumalai, R. S.; Chan, K. C.; Prieto, D. A.; Issaq, H. J.; Conrads, T. P.; Veenstra, T. D. Characterization of the Low Molecular Weight Human Serum Proteome. *Mol. Cell. Proteomics* **2003**, *2*, 1096–1103.
42. Heinrich, M. C.; Corless, C. L.; Duensing, A.; McGreevey, L.; Chen, C.; Joseph, N.; Singer, S.; Griffith, D. J.; Haley, A.; Town, A.; *et al.* PDGFRA Activating Mutations in Gastrointestinal Stromal Tumors. *Science* **2003**, *299*, 708–710.
43. Baxter, E. J.; Hochhaus, A.; Bolufer, P.; Reiter, A.; Fernandez, J. M.; Senent, L.; Cervera, J.; Moscardo, F.; Sanz, M. A.; Cross, N. C. P. The t(4;22)(q12;q11) in Atypical Chronic Myeloid

Leukaemia Fuses BCR to PDGFRA. *Hum. Mol. Genet.* **2002**, *11*, 1391–1397.
44. Yu, J.; Ustach, C.; Kim, H. R. Platelet-Derived Growth Factor Signaling and Human Cancer. *J. Biochem. Mol. Biol.* **2003**, *36*, 49–59.
45. Deng, Z. J.; Liang, M.; Toth, I.; Monteiro, M. J.; Minchin, R. F. Molecular Interaction of Poly(acrylic acid) Gold Nanoparticles with Human Fibrinogen. *ACS Nano* **2012**, *6*, 8962–8969.
46. Gagner, J. E.; Lopez, M. D.; Dordick, J. S.; Siegel, R. W. Effect of Gold Nanoparticle Morphology on Adsorbed Protein Structure and Function. *Biomaterials* **2011**, *32*, 7241–7252.